# HIGH TEMPERATURE DEFORMATION

# OF DISPERSION STRENGTHENED ALUMINUM ALLOYS

E. Arzt and J. Rösler

Max-Planck-Institut für Metallforschung
Institut für Werkstoffwissenschaften
Seestraße 92, D-7000 Stuttgart 1, W. Germany

## Abstract

This paper describes the characteristic features of high temperature deformation in dispersion-strengthened materials. It focusses on "reaction-milled" aluminum alloys containing oxide and carbide dispersoids: the microstructure of such alloys has been studied by TEM, and the creep properties have been measured at 573 - 773 K in a fine and coarse-grained condition. Recent micromechanistic models for the effect of small dispersoids on the high temperature creep properties are described. The experimental results are then interpreted in the light of a new model-based constitutive equation and compared with those of other dispersion-strengthened materials. Requirements for optimum high-temperature performance of such alloys, including an optimized grain structure, are discussed.

Dispersion Strengthened Aluminum Alloys
Edited by Y.-W. Kim and W.M. Griffith
The Minerals, Metals & Materials Society, 1988

## Introduction

Dispersion strengthening is an efficient way of raising the temperature capability of metallic materials. It has been shown for numerous alloys systems that the natural tendency of metals to soften with increasing temperature is counteracted by the presence of hard dispersoid particles whose volume fraction is usually of the order of only some percent. In mechanistic terms, these dispersoids act as barriers to dislocation motion, even at temperatures close to the melting point. The dispersoids, which must be thermally stable and insoluble in the matrix, can be incorporated by powder-metallurgical processes ("mechanical alloying"). Successful examples of the realization of this principle are dispersion-strengthened superalloys (Ni and Fe basis), whose useable service temperatures can be up to 90 % of the absolute melting points, see e.g. (1).

Compared to these developments, the high-temperature capability of aluminum-base materials has not been exploited up to now, although many important applications for such materials can be envisaged. Because of the low solubility of other elements in aluminum, particle dispersions can be readily produced by precipitation reactions. However, such dispersions are generally not ideal from a thermodynamic point-of-view: while the precipitates lead to high room-temperature strength, they tend to lose their effectiveness at elevated temperatures because of ageing. After early suggestions by E. Schmid (2) to incorporate hard, insoluble particles, this principle was first used in the fifties in $Al_2O_3$-strengthened aluminum developed by Alusuisse (3-5). This material, which has come to be known as "SAP", was produced by milling Al powder under oxidizing conditions, and subsequent compaction by extrusion. High price, low ductility and poor reproducibility of properties prevented wide-spread application of SAP.

Methods of dispersing stable particles in aluminum by mechanical means were taken up again in the seventies by J. Benjamin ("Mechanical Alloying", e.g. (6)) and G. Jangg ("Reaction Milling", see e.g. (7)). In both processes, powders are ground, generally in attritors; in addition to oxide particles from surface oxides on the powder particles, dispersoid particles are produced in the material by reaction with an organic lubricant or fine carbon black, respectively.

The focus of the experimental work described in this paper is on dispersion-strengthened aluminum alloys produced by "Reaction Milling". The microstructure of these materials was studied by transmission electron microscopy, and the high-temperature creep properties were measured at temperatures up to 500 °C (773 K). The results exhibit all the characteristic features of dispersion-strengthened materials; they will be discussed in the larger context of dispersion strengthening in general: recent developments in the theory of dispersion strengthening at high temperatures will be described and the data will also be compared with those of other dispersion-strengthened materials. Finally, requirements for optimum behavior at very high temperatures will be identified and discussed in relation to possible future aluminum alloys for high-temperature use.

## Microstructure of Dispersion-Strengthened Aluminium Alloys Procuded by "Reaction Milling"

In comparison to conventional aluminum alloys, reaction-milled material exhibits several microstructural features which are due to the special processing route and the relatively large amount of second phase. In principle, the processing encompasses the following steps: powder atomization, powder milling with addition of carbon black, heat treatment, cold compaction, de-

gassing, and hot extrusion (for a recent review of the process see (8)). The alloys studied differed in volume fraction of C added during milling (see Table I); for comparison, an alloy variant with no carbon added ("AlCO") and a solute strengthened matrix material ("AlMg4C1") were also included. Some results of the microstructural investigations are reported in this section; for further details the reader is referred to a forthcoming publication (9).

Table I. Details of AlC Alloys Investigated
(Tradename DISPAL, Krebsöge and Erbslöh Aluminium)

| Material | C | O[a] | Mg | total $f_v$ [e] | grain size [b], µm | GAR[c] |
|---|---|---|---|---|---|---|
| AlC2 | 2 | 1 | – | 10 | 0.7 (0.5) | 1.6 |
| AlC1 | 1 | 1 | – | 6 | 1.2 (0.8) | 1.8 |
| AlMg4C1 | 1 | 1 | 4 | 6 | (d) | (d) |
| AlCO | – | 1 | – | 2 | 1.9 (2.5) | 2.1 |

a estimated weight percentage
b theoretical value (eq. 1) in parenthesis
c GAR = grain aspect ratio
d not determined
e estimated total volume fraction of dispersoid

## Investigation of the Dispersoid Particles

Alumina Dispersoids. In AlCO the only dispersoid present is aluminum oxide, which originates from the powder particle surface. The TEM micrograph in fig. 1 shows that only a certain fraction of the particles is distributed homogeneously in the matrix, whereas another particle population is aligned parallel to the extrusion direction. This latter population is probably incorporated in the material during milling as amorphous surface layers of oxide/hydroxide. Since these amorphous layers are believed to be ductile (10, 11), their breaking up and distribution is incomplete; the remaining oxide films are then fractured and aligned during hot extrusion.

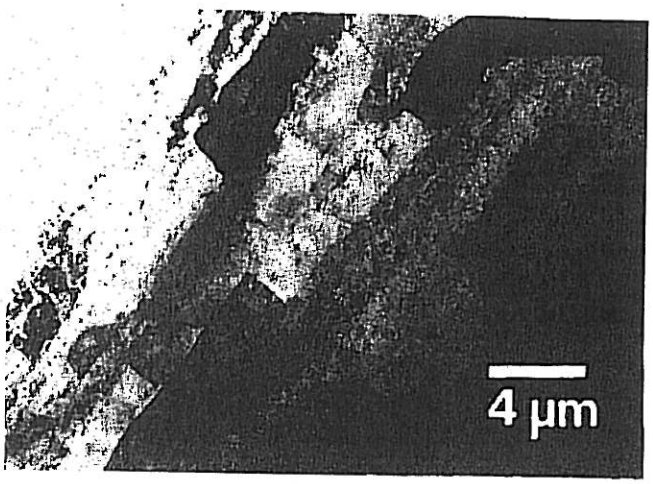


Figure 1 – TEM micrograph of alloy AlCO, longitudinal section, showing predominantly the alumina dispersoid aligned in the extrusion direction. The grains are elongated with an average aspect ratio of about 2.1.

The shape of the alumina dispersoids is generally equiaxed, with a mean diameter of about 50 nm (fig. 2a). From selected area diffraction patterns, the crystal structure can be narrowed down to $\gamma$- or $\eta$-$Al_2O_3$ (fig. 2b). Because of almost identical lattice spacings, we cannot distinguish unambiguously between these two modifications; in the literature the occurrence of $\gamma$-$Al_2O_3$(12-14), and sometimes of $\eta$-$Al_2O_3$(15) and $\alpha$-$Al_2O_3$(16) is reported.

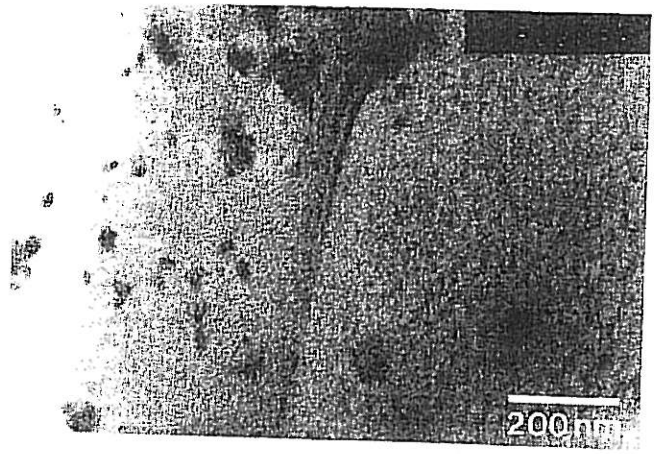


Figure 2a - TEM micrograph of alumina dispersoids in alloy AlCO.

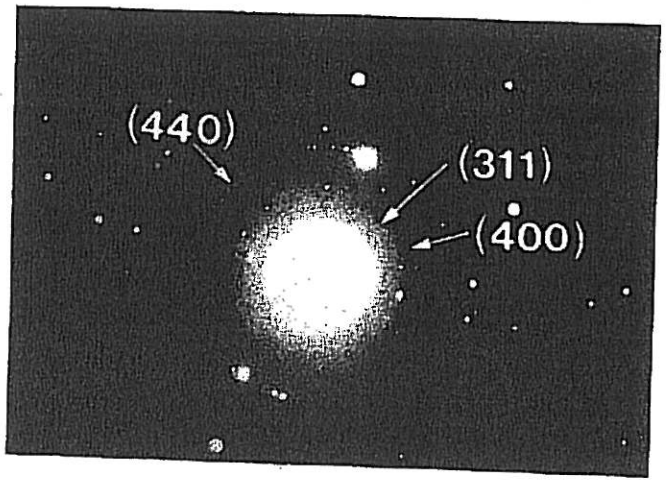


Figure 2b - Diffraction pattern, identifying the dispersoids as $\gamma$- or $\eta$-$Al_2O_3$.

Carbide Dispersoids. When carbon is added during powder milling (alloys AlC1, AlC2), then characteristic platelike dispersoids form on appropriate heat treatment (fig. 3a). These dispersoids can be identified as $Al_4C_3$ by electron diffraction (fig. 3b). Their morphology may be attributed to the tendency of $Al_4C_3$ to fracture along the basal plane (17). High resolution imaging (fig. 4) shows in fact that the (003) basal planes are oriented parallel to the particle contour. The carbide dispersoids are, like the oxides, incoherent with the matrix and do not exhibit preferrred orientations. Their characteristic thickness is about 20 nm, their mean length about 80 nm. The distribution appears to be more homogeneous than that of the oxide dispersoids.

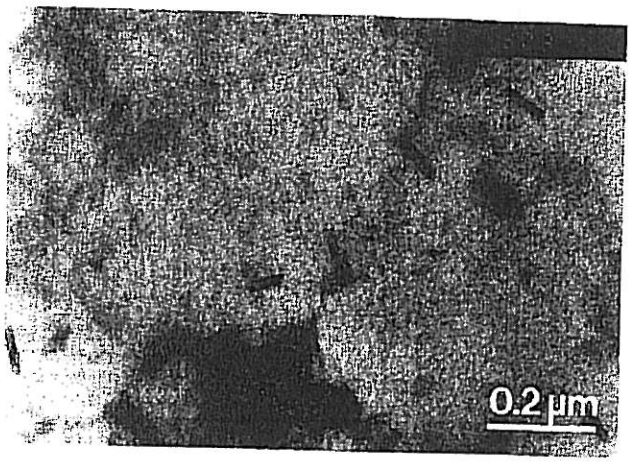


Figure 3a - TEM micrograph of carbide dispersoids in alloy AlC2

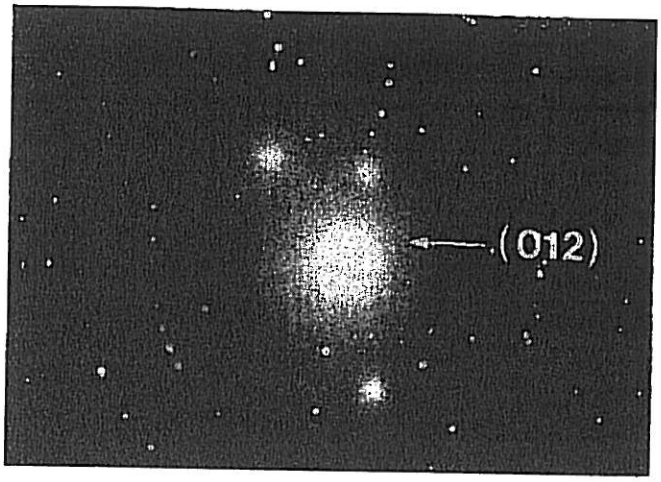


Figure 3b - Diffraction pattern, identifying $Al_4C_3$.

The shape of the alumina dispersoids is generally equiaxed, with a mean diameter of about 50 nm (fig. 2a). From selected area diffraction patterns, the crystal structure can be narrowed down to $\gamma$- or $\eta$-$Al_2O_3$ (fig. 2b). Because of almost identical lattice spacings, we cannot distinguish unambiguously between these two modifications; in the literature the occurrence of $\gamma$-$Al_2O_3$(12–14), and sometimes of $\eta$-$Al_2O_3$(15) and $\alpha$-$Al_2O_3$(16) is reported.

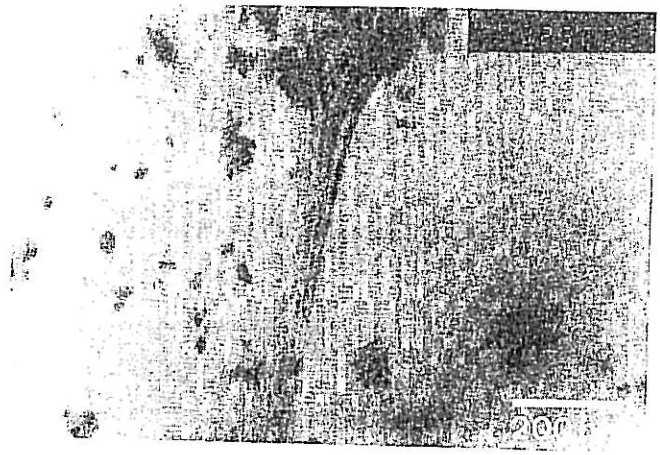

Figure 2a – TEM micrograph of alumina dispersoids in alloy AlCO.

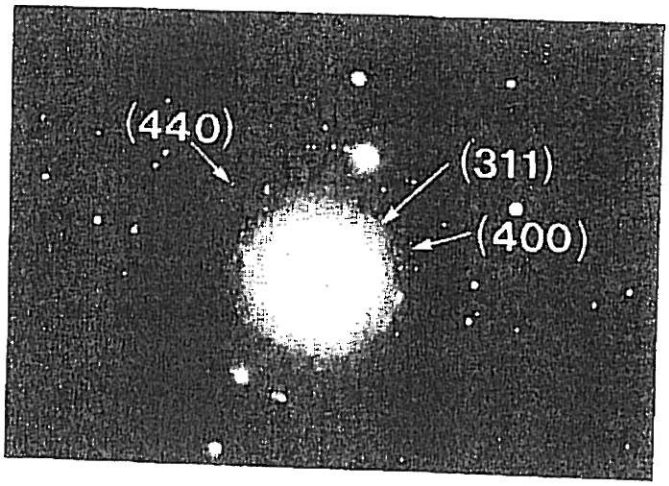


Figure 2b – Diffraction pattern, identifying the dispersoids as $\gamma$- or $\eta$-$Al_2O_3$.

Carbide Dispersoids. When carbon is added during powder milling (alloys AlC1, AlC2), then characteristic platelike dispersoids form on appropriate heat treatment (fig. 3a). These dispersoids can be identified as $Al_4C_3$ by electron diffraction (fig. 3b). Their morphology may be attributed to the tendency of $Al_4C_3$ to fracture along the basal plane (17). High resolution imaging (fig. 4) shows in fact that the (003) basal planes are oriented parallel to the particle contour. The carbide dispersoids are, like the oxides, incoherent with the matrix and do not exhibit preferrred orientations. Their characteristic thickness is about 20 nm, their mean length about 80 nm. The distribution appears to be more homogeneous than that of the oxide dispersoids.

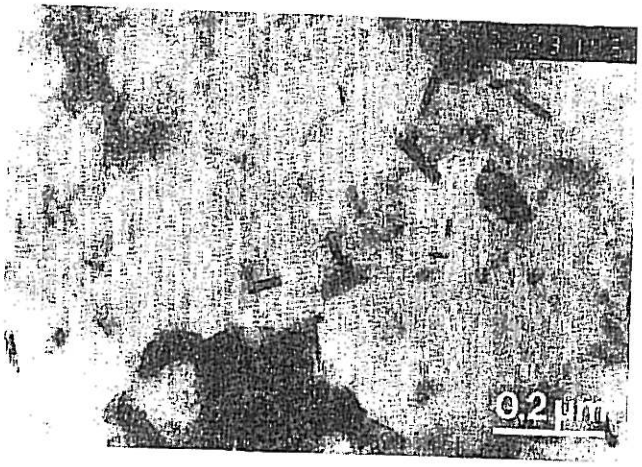


Figure 3a - TEM micrograph of carbide dispersoids in alloy AlC2

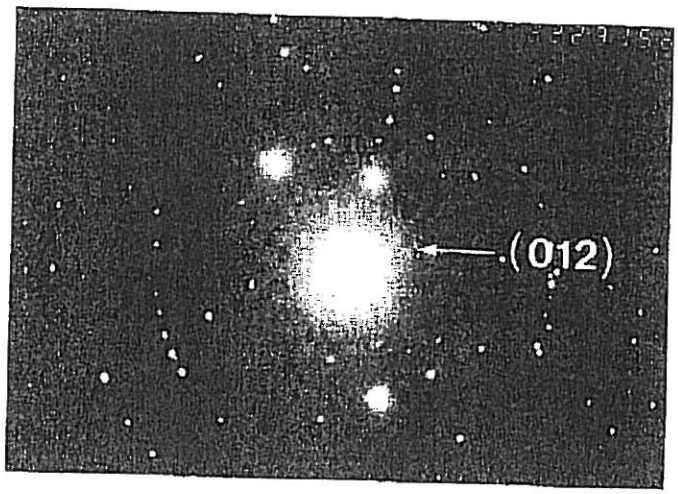


Figure 3b – Diffraction pattern, identifying $Al_4C_3$.

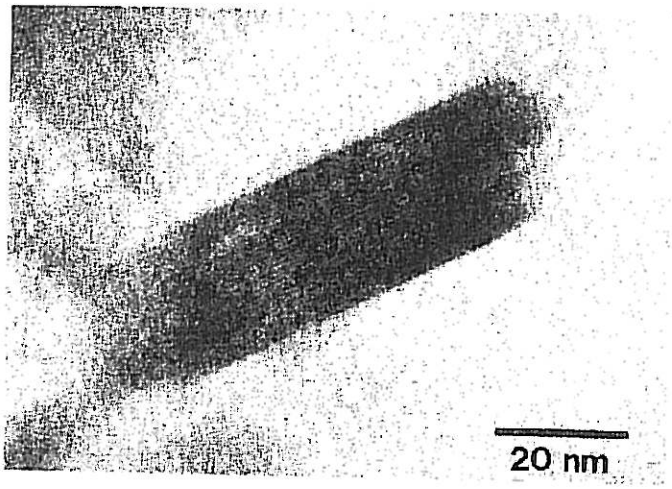


Figure 4 - High resolution TEM micrograph of a carbide dispersoid.

Magnesia Dispersoids. The microstructure and a diffraction pattern of the Mg-containing alloy AlMg4C1 are shown in fig. 5. In agreement with (16), MgO, which is thermodynamically more stable, is found to replace $Al_2O_3$. Because the oxygen content of the alloy is about 1 wt.%, 1.5 wt.% Mg is required to form MgO and only 2.5 wt.% Mg is left in solid solution. The dispersoid volume fraction is not significantly changed, as 1 % of oxygen gives about 1.8 vol.% $Al_2O_3$ or 1.9 vol.% MgO.

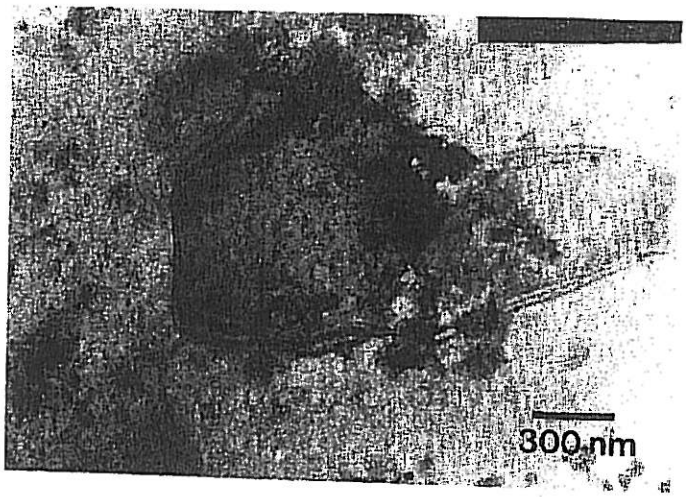


Figure 5a - TEM micrograph of magnesia dispersoids in alloy AlMg4C1.

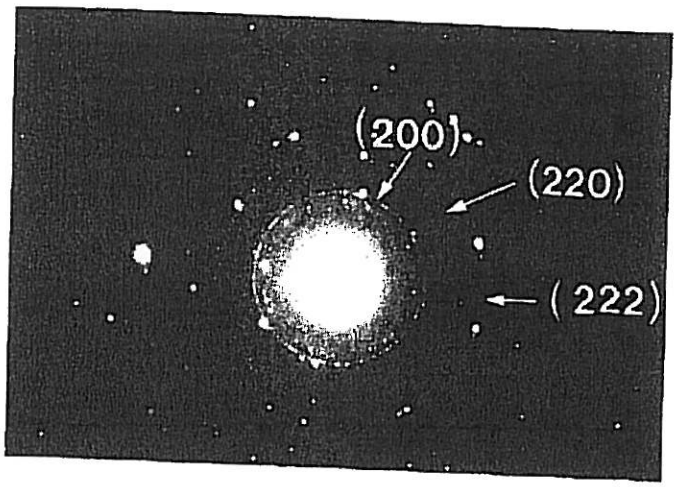


Figure 5b – Diffraction pattern.

Grain Structure

Besides the dispersoid particles, the grain structure is also important for the mechanical behavior. A characteristic feature of all reaction-milled alloys is their fine sub-micron grain size (fig. 6), which contributes significantly to the room-temperature strength. The grain size correlates with the total dispersoid content (table I), indicating that grain growth is controlled by the dispersoid particles. A rough estimate for the Zener grain size d is

$$d \sim \frac{2R}{f_v} \qquad (1)$$

where 2R is the particle size and $f_v$ the volume fraction of dispersoid. These values are in reasonable agreement with grain sizes, measured on planes perpendicular to the extrusion direction, for the three different volume fractions.

In a plane parallel to the extrusion axis, the grains have a slightly elongated shape (figs. 6b and 1), with the grain aspect ratio (GAR) depending on dispersoid volume fraction (table I): while alloy A1C2 consists of only weakly elongated grains (GAR ~ 1.6), A1CO (which was milled without any addition of carbon) exhibits a more elongated grain stucture (GAR ~ 2.1). This dependence arises due to the more strongly aligned oxide particles in A1CO, which act as barriers to grain boundary motion perpendicular to the extrusion axis. The grains are believed to form by dynamic recrystallization during hot extrusion, which is also supported by the low dislocation density in as-extruded material.

Figure 4 - High resolution TEM micrograph of a carbide dispersoid.

Magnesia Dispersoids. The microstructure and a diffraction pattern of the Mg-containing alloy AlMg4Cl are shown in fig. 5. In agreement with (16), MgO, which is thermodynamically more stable, is found to replace $Al_2O_3$. Because the oxygen content of the alloy is about 1 wt.%, 1.5 wt.% Mg is required to form MgO and only 2.5 wt.% Mg is left in solid solution. The dispersoid volume fraction is not significantly changed, as 1 % of oxygen gives about 1.8 vol.% $Al_2O_3$ or 1.9 vol.% MgO.




TEM micrograph of magnesia dispersoids in alloy AlMg4Cl.

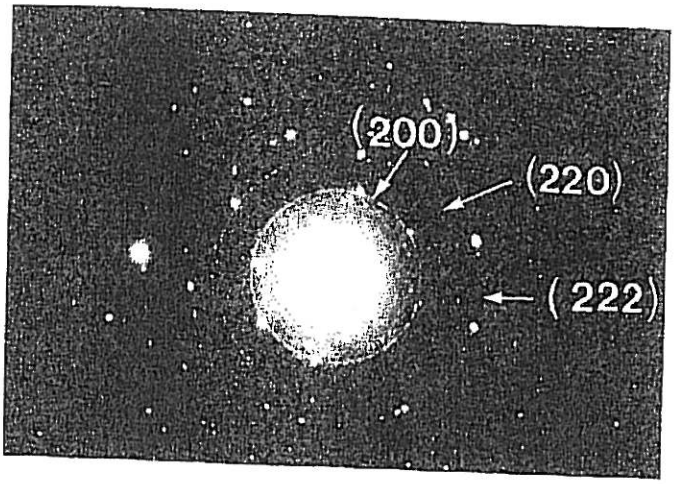


Figure 5b - Diffraction pattern.

Grain Structure

Besides the dispersoid particles, the grain structure is also important for the mechanical behavior. A characteristic feature of all reaction-milled alloys is their fine sub-micron grain size (fig. 6), which contributes significantly to the room-temperature strength. The grain size correlates with the total dispersoid content (table I), indicating that grain growth is controlled by the dispersoid particles. A rough estimate for the Zener grain size d is

$$d \sim \frac{2R}{f_v} \qquad (1)$$

where 2R is the particle size and $f_v$ the volume fraction of dispersoid. These values are in reasonable agreement with grain sizes, measured on planes perpendicular to the extrusion direction, for the three different volume fractions.

In a plane parallel to the extrusion axis, the grains have a slightly elongated shape (figs. 6b and 1), with the grain aspect ratio (GAR) depending on dispersoid volume fraction (table I): while alloy A1C2 consists of only weakly elongated grains (GAR ~ 1.6), A1CO (which was milled without any addition of carbon) exhibits a more elongated grain stucture (GAR ~ 2.1). This dependence arises due to the more strongly aligned oxide particles in A1CO, which act as barriers to grain boundary motion perpendicular to the extrusion axis. The grains are believed to form by dynamic recrystallization during hot extrusion, which is also supported by the low dislocation density in as-extruded material.

Figure 6 - TEM micrographs of alloy A1C2:
a) transverse section.

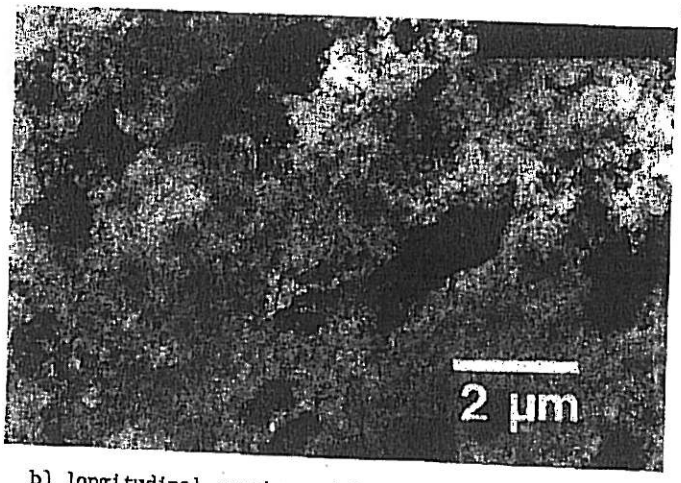


b) longitudinal section, with extrusion axis along diagonal from lower left to upper right corner.

In the literature the fine grains in similar alloys are sometimes identified as subgrains (12). In the present study, subgrain boundaries, which divide elongated grains into smaller entities, were observed only occasionally (fig. 7). A full analysis of misorientations between adjacent grains was not conducted, but subgrain boundaries can be distinguished from grain boundaries by the presence of typical dislocation arrays. The materials with higher volume fractions of dispersoid, in which the grains themselves are very small, contain practically no subgrains.

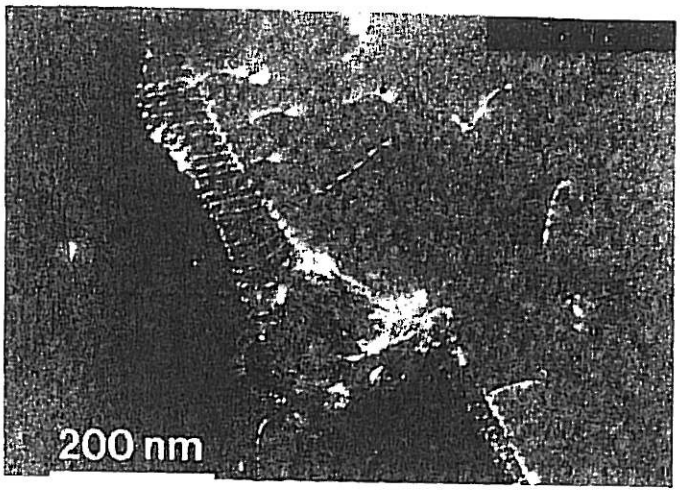


Figure 7 – Subgrain boundary composed of discrete lattice dislocations in alloy AlC0.

## High Temperature Creep Behavior

In this section the results of creep tests on alloys AlC2, AlC1, AlMg4C1, and AlC0 are presented. In order to clarify the effect of grain boundaries, creep measurements on grain-coarsened materials were conducted also. An interpretation of the "anomalous" stress and temperature dependencies is attempted in the frame of the current "threshold stress" concept. The description of recent micromechanistic modelling is postponed to the following section.

### Experimental Creep Data and TEM Results

The high temperature creep properties of the AlC alloys were measured at 573, 673, and 773 K. Compression tests at constant displacement rates corresponding to strain rates between $10^{-7}$ and $10^{-3}$ $s^{-1}$ were conducted in an electromechanical testing machine, equipped with an RF induction coil heating. The load response, which approached a steady state after a short initial period, was recorded and the load at steady state was converted into a creep stress. The stress direction was always parallel to the extrusion axis.

In general, the strain rate $\dot{\epsilon}$ of a material deforming by creep can be described by a semi-empirical power-law function of the applied stress $\sigma$ (18):

$$\dot{\epsilon} = A \cdot \frac{D_V E b}{k_B T} \left(\frac{\sigma}{E}\right)^n \qquad (2)$$

where n is the "stress exponent" (typically 3 to 7 for dispersoid-free alloys), $D_V$ is the volume diffusivity, E Young's modulus, b the magnitude of a Burgers vector, $k_B$ Boltzmann's constant, T the absolute temperature, and A a

Figure 6 - TEM micrographs of alloy AlC2:
a) transverse section.

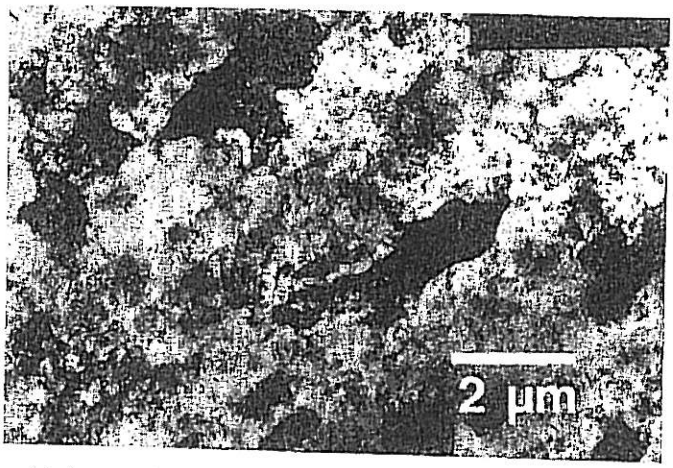


b) longitudinal section, with extrusion axis along diagonal from lower left to upper right corner.

In the literature the fine grains in similar alloys are sometimes identified as subgrains (12). In the present study, subgrain boundaries, which divide elongated grains into smaller entities, were observed only occasionally (fig. 7). A full analysis of misorientations between adjacent grains was not conducted, but subgrain boundaries can be distinguished from grain boundaries by the presence of typical dislocation arrays. The materials with higher volume fractions of dispersoid, in which the grains themselves are very small, contain practically no subgrains.

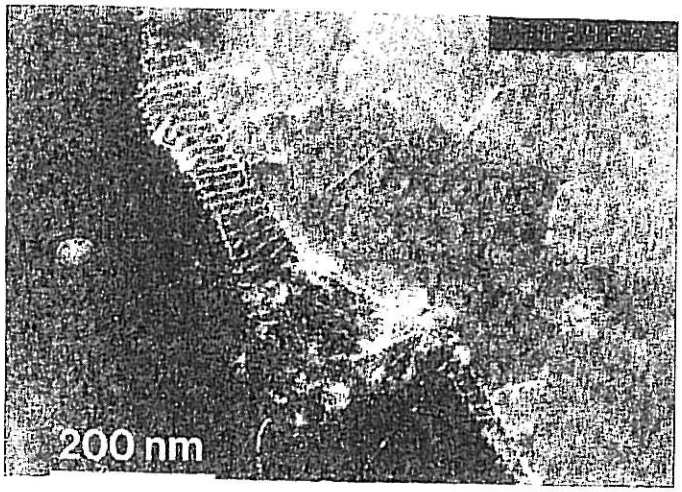


Figure 7 - Subgrain boundary composed of discrete lattice dislocations in alloy AlCO.

## High Temperature Creep Behavior

In this section the results of creep tests on alloys AlC2, AlC1, AlMg4C1, and AlCO are presented. In order to clarify the effect of grain boundaries, creep measurements on grain-coarsened materials were conducted also. An interpretation of the "anomalous" stress and temperature dependencies is attempted in the frame of the current "threshold stress" concept. The description of recent micromechanistic modelling is postponed to the following section.

### Experimental Creep Data and TEM Results

The high temperature creep properties of the AlC alloys were measured at 573, 673, and 773 K. Compression tests at constant displacement rates corresponding to strain rates between $10^{-7}$ and $10^{-3}$ $s^{-1}$ were conducted in an electromechanical testing machine, equipped with an RF induction coil heating. The load response, which approached a steady state after a short initial period, was recorded and the load at steady state was converted into a creep stress. The stress direction was always parallel to the extrusion axis.

In general, the strain rate $\dot{\varepsilon}$ of a material deforming by creep can be described by a semi-empirical power-law function of the applied stress $\sigma$ (18):

$$\dot{\varepsilon} = A \cdot \frac{D_V E b}{k_B T} \left(\frac{\sigma}{E}\right)^n \qquad (2)$$

where n is the "stress exponent" (typically 3 to 7 for dispersoid-free alloys), $D_V$ is the volume diffusivity, E Young's modulus, b the magnitude of a Burgers vector, $k_B$ Boltzmann's constant, T the absolute temperature, and A a

dimensionless material constant. As is common practice, the test results are plotted in fig. 8 in temperature-compensated form $\dot{\varepsilon}/D_v$ vs. $\sigma/E$ (the remaining temperature dependence of E/T can always be neglected in this context).

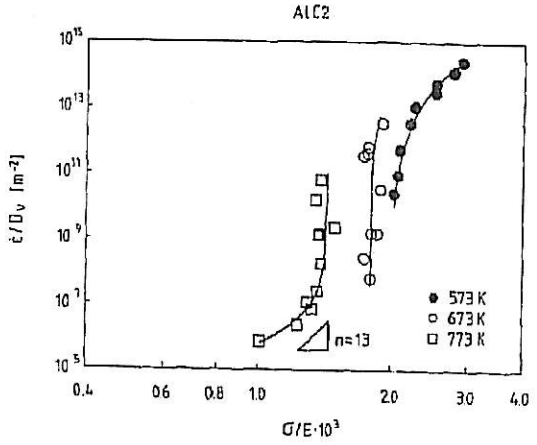


Figure 8 - Compression creep results, plotted in compensated form $\dot{\varepsilon}/D_v$ vs. $\sigma/E$. $D_v = 1.7 \times 10^{-4} \exp(-Q_v/RT)$ m$^2$/s, with $Q_v$ = 142 kJ/mole, and E = 58.5 GPa, 54.9 GPa and 51.2 GPa at 573, 673 and 773K, respectively.
a) alloy AlC2

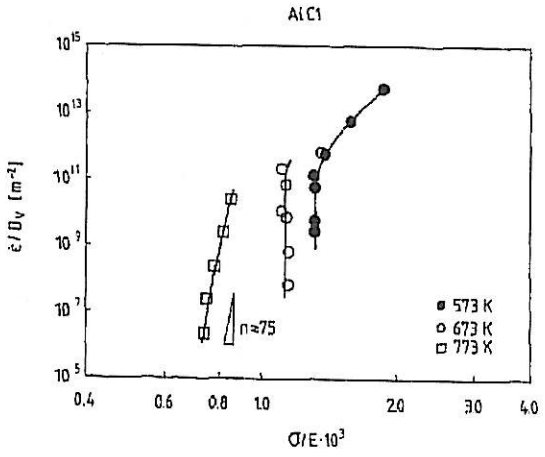


b) alloy AlC1

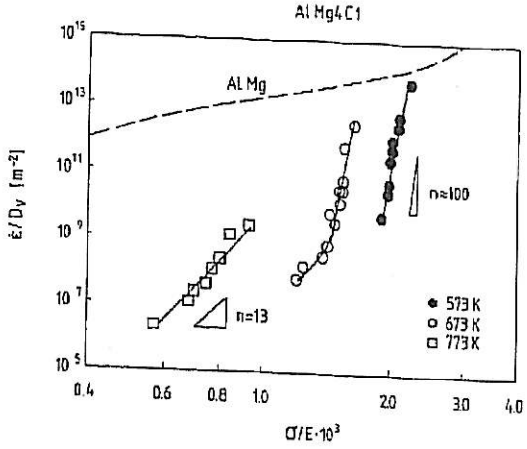


c) alloy AlMg4C1

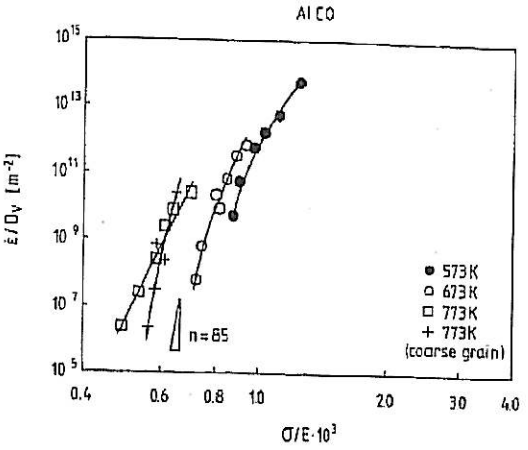


d) alloy AlCO

The following characteristics, which are typical of many dispersion-strengthened materials, can be found in fig. 8. All alloys have a region of extremely high stress sensitivity, with stress exponents $n > 50$. The creep rates are many orders of magnitude lower than in pure aluminum. TEM micrographs confirm that the mechanism controlling creep strength in this region is the interaction between single lattice dislocations and dispersoid particles (fig. 9a); the dislocation density is low and no dislocation networks are observed. At higher creep rates ($\dot{\varepsilon}/D_V > 10^{12}$ m$^{-2}$), the stress sensitivity decreases progressively; here the dislocation density increases and networks, which are stabilized by larger dispersoid particles, are formed (fig. 9b). The creep strength is still considerably better than in pure alu-

minum. At low strain rates and high temperatures (low $\dot{\varepsilon}/D_V$) the stress exponents decrease, too. This effect is especially pronounced in alloys AlC2 and AlMg4C1, which exhibit a very fine grain structure, but is also evident in AlCO and AlC1. As will be discussed below, this is a consequence of grain boundary processes which become dominant at high temperatures.

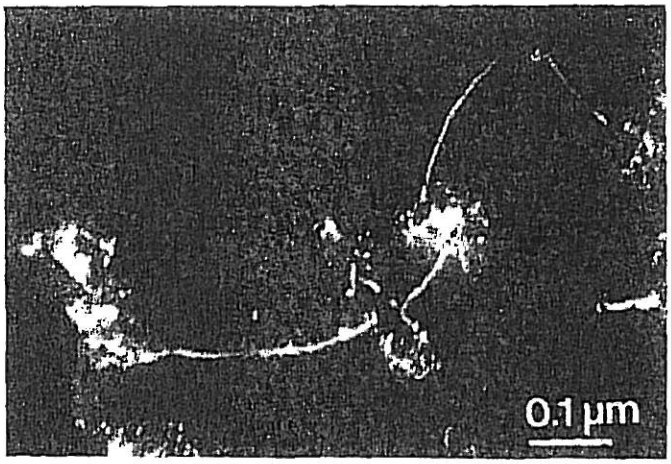


Figure 9 - TEM micrographs of crept specimens:
a) at intermediate strain rates (high n-region), showing interaction of a single dislocation with a carbide dispersoid in alloy AlC2.

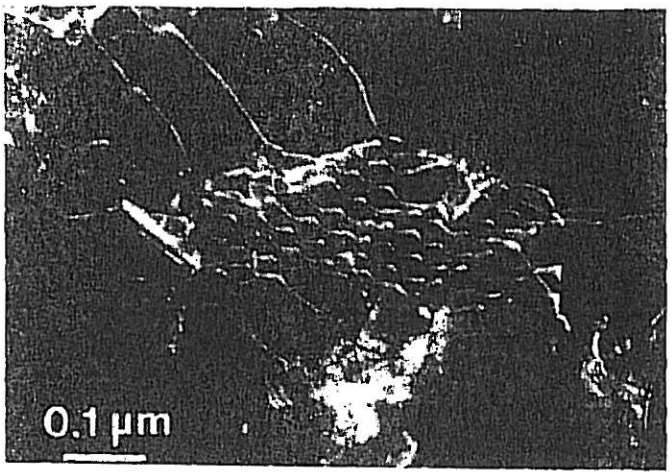


b) at higher strain rates, with network formation in alloy AlC2.

Another important characteristic relates to the temperature dependence of the creep rate. The fact that the data for different temperatures do not superimpose on the temperature-compensated plot in fig. 8 indicates that the

activation energy is higher than that for volume diffusion. A simple Arrhenius plot log $\dot{\varepsilon}$ vs. 1/T gives an apparent activation energy of 537 kJ/mole for alloy AlCO, compared to 142 kJ/mole for volume diffusion in aluminum (19). Addition of Mg increases the temperature dependence even further.

Both the high stress and temperature dependence of the creep rates in the alloys investigated are typical of dispersion-strengthened high-temperature alloys. It is emphasized that stress exponents of the order of 50 and activation energies far beyond that for diffusion can have only doubtful physical meaning. In order to explain the behavior of such materials in a satisfactory way, new concepts have been put forward which will be described further below.

Grain-Coarsened Material

We turn first to the region of reduced stress sensitivity at low $\dot{\varepsilon}/D_V$. Similarly shaped creep plots have been attributed to the dissolution of dispersoids in TD-NiCr (21), to the effect of small-grain pockets in an otherwise coarse-grained Ni-Cr-$Y_2O_3$ alloy (22), and to the increasing deformability of intermetallic dispersoids in rapidly solidified Al-Fe-Ce (23). In the fine-grained alloys investigated, the grain boundaries would be the most likely cause for this weakening effect. In order to test this hypothesis, some material was subjected to a grain-coarsening treatment and then creep tested.

Uniform recrystallization to a coarse grain structure could be achieved only in the alloy AlCO, after cold reduction from 12 to 3 mm diameter and annealing at temperatures around 550 °C. The resulting grains have typical dimensions of 3 by 0.2 mm and an aspect ratio of about 15 (fig. 10). The creep data at 773 K (also shown in fig. 8) give an increased stress exponent $n \approx 60$ and a consistently higher creep strength than in the fine-grained state. Thus, the reduced stress sensitivity in the fine-grained material can be attributed unambiguously to the effect of grain boundaries. As a consequence, when isolating the influence of dispersoids on the grain strength, only the regions of high stress sensitivity should be considered.

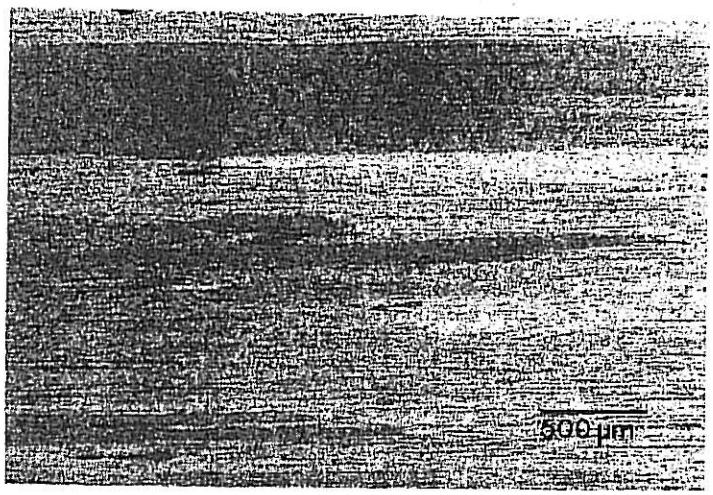


Figure 10 - Coarse elongated grain structure of alloy AlCO after secondary recrystallization (longitudinal section)

minum. At low strain rates and high temperatures (low $\dot{\varepsilon}/D_V$) the stress exponents decrease, too. This effect is especially pronounced in alloys AlC2 and AlMg4C1, which exhibit a very fine grain structure, but is also evident in AlC0 and AlC1. As will be discussed below, this is a consequence of grain boundary processes which become dominant at high temperatures.

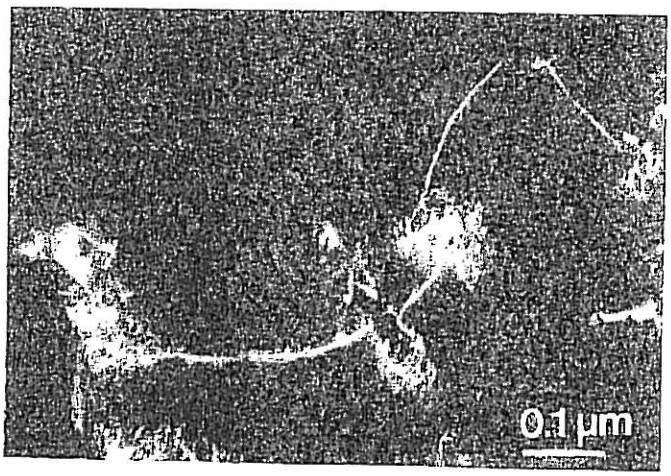


Figure 9 - TEM micrographs of crept specimens:
a) at intermediate strain rates (high n-region), showing interaction of a single dislocation with a carbide dispersoid in alloy AlC2.

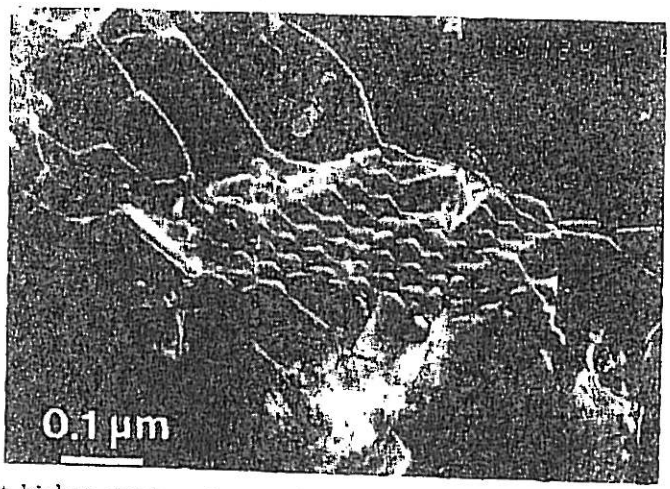


b) at higher strain rates, with network formation in alloy AlC2.

Another important characteristic relates to the temperature dependence of the creep rate. The fact that the data for different temperatures do not superimpose on the temperature-compensated plot in fig. 8 indicates that the

activation energy is higher than that for volume diffusion. A simple Arrhenius plot log $\dot{\varepsilon}$ vs. 1/T gives an apparent activation energy of 537 kJ/mole for alloy AlCO, compared to 142 kJ/mole for volume diffusion in aluminum (19). Addition of Mg increases the temperature dependence even further.

Both the high stress and temperature dependence of the creep rates in the alloys investigated are typical of dispersion-strengthened high-temperature alloys. It is emphasized that stress exponents of the order of 50 and activation energies far beyond that for diffusion can have only doubtful physical meaning. In order to explain the behavior of such materials in a satisfactory way, new concepts have been put forward which will be described further below.

Grain-Coarsened Material

We turn first to the region of reduced stress sensitivity at low $\dot{\varepsilon}/D_V$. Similarly shaped creep plots have been attributed to the dissolution of dispersoids in TD-NiCr (21), to the effect of small-grain pockets in an otherwise coarse-grained Ni-Cr-$Y_2O_3$ alloy (22), and to the increasing deformability of intermetallic dispersoids in rapidly solidified Al-Fe-Ce (23). In the fine-grained alloys investigated, the grain boundaries would be the most likely cause for this weakening effect. In order to test this hypothesis, some material was subjected to a grain-coarsening treatment and then creep tested.

Uniform recrystallization to a coarse grain structure could be achieved only in the alloy AlCO, after cold reduction from 12 to 3 mm diameter and annealing at temperatures around 550 °C. The resulting grains have typical dimensions of 3 by 0.2 mm and an aspect ratio of about 15 (fig. 10). The creep data at 773 K (also shown in fig. 8) give an increased stress exponent $n \approx 60$ and a consistently higher creep strength than in the fine-grained state. Thus, the reduced stress sensitivity in the fine-grained material can be attributed unambiguously to the effect of grain boundaries. As a consequence, when isolating the influence of dispersoids on the grain strength, only the regions of high stress sensitivity should be considered.

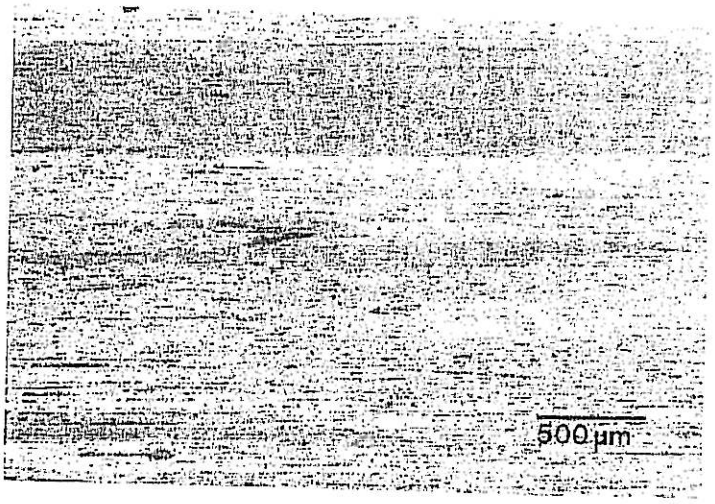


Figure 10 - Coarse elongated grain structure of alloy AlCO after secondary recrystallization (longitudinal section)

Threshold Stress Concept

The high stress and temperature dependencies of the creep rates in dispersion strengthened materials are "anomalous" in the sense that eq. 2, which is a valid constitutive equation for dispersion-free materials, fails to describe the behavior of dispersion-strengthened alloys. One possibility to rationalize the high stress sensitivity is to modify eq. 2 by introducing a so-called "threshold stress", below which creep is considered to be negligible, e.g. (20):

$$\dot{\varepsilon} = A \frac{D_V E b}{k_B T} \left(\frac{\sigma - \sigma_{th}}{E}\right)^n \qquad (3)$$

In this way, more reasonable n values, typical of dispersion-free materials, are usually obtained.

Threshold stress data were extracted from the creep data in fig. 8 by replotting $\dot{\varepsilon}^{1/n}$ vs. $\sigma$, with n = 4.4 as for pure aluminum (19), and extrapolating to $\dot{\varepsilon} = 0$. They are listed in table II.

Table II: Threshold stresses as a function of temperature

| Alloy | 573 K | 673 K | 773 K |
|---|---|---|---|
| AlC2 | 111 | 99 | 70 |
| AlC1 | 70 | 59 | 38 |
| AlMg4C1 | 110 | 75 | (29)[a] |
| AlC0 | 47 | 36 | 30[b] (25)[a] |

a data with onset of grain boundary effects in parenthesis
b grain-coarsened material

In fig. 11 the threshold stresses of several dispersion-strengthened materials are plotted as $\sigma_{th}/\sigma_{0r}$ vs. $T/T_m$, where $\sigma_{0r}$ is the estimated Orowan stress and $T_m$ the absolute melting (or solidus) temperature. In order to compare the threshold stress data of the AlC alloys, the values of the Orowan stresses would have to be known. Because of the complicated morphology of the carbide dispersoids, their spacing is subject to large experimental errors. We have therefore included only the data for AlC0, for which the Orowan stress can be estimated from the room temperature yield stress in the coarse-grained condition ($\sigma_{0r} \approx 75$ MPa).

In all cases the threshold stress is below the Orowan stress, and decreases with increasing temperature. The coincidence of the data points from the different alloy systems suggests that the Orowan stress is a useful normalizing parameter and that similar mechanisms are responsible for the creep strength in these alloys.

The high apparent activation energy can also be rationalized by the threshold concept if the temperature dependence of the threshold stress is considered. For example, at a stress just below the threshold stress a temperature increase will suddenly promote creep as the threshold falls below the applied stress. Thus a high "apparent" activation energy for creep results. With reference to eq. 3, the "true" value of the activation energy can only be determined by plotting log $(d\dot{\varepsilon}^{1/n}/d\sigma)$ vs 1/T. In this way we obtain Q = 123 kJ/mole, which is in acceptable agreement with the value $Q_V$ for volume diffusion. Similar analyses for other dispersion-strengthened materials lead to the same close agreement, even in cases where the "apparent" activation energy amounts to three or four times $Q_V$.

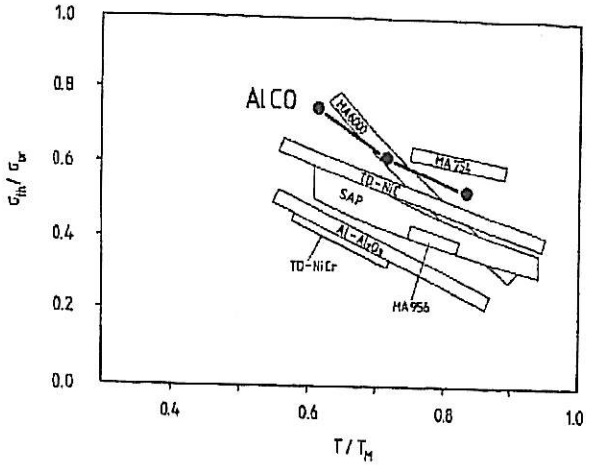


Figure 11 - Threshold stress (normalized with respect to the estimated Orowan stress) as a function of homologous temperature for ALCO, and a number of other Al-, Fe- and Ni-base dispersion-strengthened alloys.

In summary, the threshold stress concept has considerable merit for formal rationalization of the creep behavior in dispersion-strengthened alloys. It does not touch on the fundamental questions: can a "true" threshold stress, below which deformation stops completely, exist; what are the mechanisms which lead to a threshold stress behavior; and, for example, why does the threshold stress depend on temperature? These questions lead to the area of micromechanistic modelling in which considerable advances appear to have been made in the recent past.

## Micromechanistic Models for the Effect of Dispersoid Particles on Creep

The justification of a threshold stress behavior in terms of dislocation theory has been a research subject over the past fifteen years, but the mechanisms of dispersion strengthening in high-temperature materials seem to have eluded a full description up to now. Early papers sought an explanation in terms of the Orowan process and its thermal activation (24). But once the threshold stresses were found to be generally lower than the Orowan stress of the particle dispersion, further models focussed on the process by which dislocations can circumvent hard particles, expecially by climbing around them. Following detailed transmission electron microscoping of this process, more attention has been paid recently to the interaction between dispersoid particles and the dislocations.

These theoretical developments are briefly summarized below. The creep behavior of dispersion-strengthened aluminum alloys is then interpreted in the light of the most recent developments in this field. Perhaps the most important result from a fundamental point-of-view is that a "true" threshold stress does not exist, but that for practical purposes - where finite strain

rates are considered - a "threshold stress behavior" is a useful approximation. These findings also lead to practical conclusions with respect to alloy design.

Dislocation Climb Models

When the dispersoid particles are considered as impenetrable glide obstacles which force the dislocations to climb a certain distance until they can continue to glide, a retardation of creep is predicted but a threshold stress behavior cannot be explained in this way (25). Only by realizing that the dislocation has to increase its line length in order to surmount the dispersoid, can a climb-related threshold stress be justified. This process has been modelled by Brown and Ham (26) and Shewfelt and Brown (27), who assumed that climb is "local"; this means that only the portion of the dislocation which is in close proximity with the particle-matrix interface undergoes climb while the remaining segment stays in the glide plane (fig. 12a). The resulting minimum threshold stress for climb is proportional to the Orowan stress:

$$\sigma_{th} = C \cdot \sigma_{Or} \approx C \cdot \frac{Gb}{l} \qquad (4)$$

with $C \approx 0.7$ for cubes (as in fig. 12a) and $C \approx 0.4$ for spheres.

While the assumption of "local" climb predicts threshold stress values of correct order-of-magnitude (see fig. 11), the postulate concerning dislocation shape in the vicinity of the dispersoid particle must be regarded as an unduly restrictive. Lagneborg (28) has argued rightly that local climb would be an extreme non-equilibrium process: the sharp bend in the dislocation at the point where it leaves the particle-matrix interface will in reality be rapidly relaxed by diffusion, leading to more "general" climb. Because the additional line length required is much reduced, only a small climb-related threshold stress would be predicted. Lagneborg's argument seems convincing; his model, however, does not treat the full kinetics of the modified climb process.

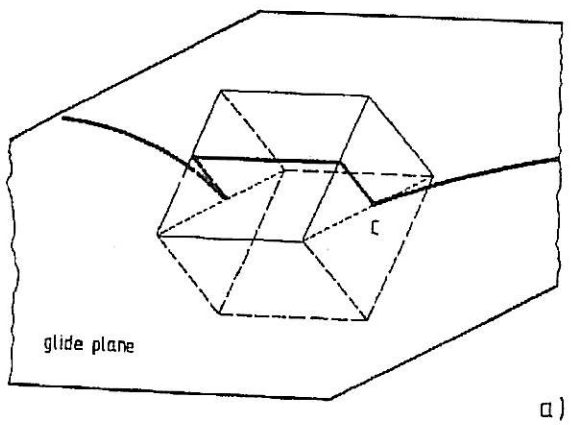


a)

Figure 12 - Dislocation geometries during climb over a simple cuboidal particle:
a) "local" climb: the sharp dislocation curvatures at "C" represent unrealistically high energies (26)

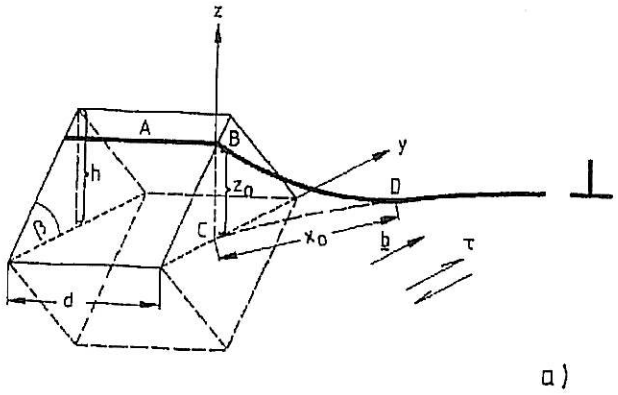


a)

b) "equilibrium" climb: the chemical potential for vacancies along the curved dislocation segment matches the chemical potential along the segment at the particle (29).

We have recently reconsidered the process of dislocation climb over cuboidal particles (29). The only assumption concerning the dislocation geometry was that of local equilibrium (fig. 12b): the chemical potential for vacancies along segment BD (which is reduced by the curvature) is set equal to the chemical potential along AB (which is negatively biased by the applied stress). This equilibrium is rapidly established by short-range diffusion, compared to the supply of new vacancies, which requires diffusion over typically one particle spacing.

Two important results emerge from this treatment of "equilibrium climb": i) the extent to which climb is localized in the vicinity of the dispersoid particle increases with applied stress, but truly "local" climb is always unstable, and ii) climb-related threshold stresses are far below experimental values. The constitutive equation for "equilibrium climb" is (29):

$$\dot{\epsilon} = \frac{2\rho G b^4 A}{k_B T\, d^3} \left(a_p D_p + \pi D_v d\ell\right) \left(\frac{\sigma-\sigma^r_{th}}{\sigma_{Or}}\right)^n \qquad (5)$$

where $A = 60 \cdot 10^{-1.9\beta} \cdot \left(\frac{d}{h}\right)^{1.6}$

$n = 3.5\, \beta^{0.3} \cdot \left(\frac{h}{d}\right)^{0.2}$

$\sigma^r_{th} = \sigma_{Or} \sin\left(\frac{2h}{\ell} \tan\beta\right)$

($\rho$ is the density of mobile dislocations, G the shear modulus, b the magnitude of a lattice Burgers vector, $k_B$ Boltzmann's constant, T the absolute temperature, d, h and $\beta$ are particle width, height and angle according to

fig. 12b, $\ell$ is the particle spacing, $a_p D_p$ is the cross section of a dislocation core times its diffusivity, $D_v$ is the volume diffusivity, $\sigma$ the applied stress, $\sigma'_{th}$ a threshold stress for "general" climb and $\sigma_{or}$ the Orowan stress.)

When the theoretical stress-dependence of the creep rate is plotted graphically, it is seen that "equilibrium climb", with a typical stress exponent of about 4, fails to predict the threshold-stress behavior of dispersion-strengthened materials. Thus, if the only effect of dispersoid particles consisted in forcing the dislocations to climb over them, they would be weak barriers to deformation at high temperatures.

We note in passing that "equilibrium climb" offers a good qualitative explanation for the (much less stress-sensitive) creep behavior of materials with coherent particles. There the climb process seems to be dominant at high temperatures. By contrast, dispersion-strengthened materials with coherent dispersoids must derive their excellent creep strength from a different mechanism.

A Model Allowing for Attractive Dispersoid-Dislocation Interaction

In the search for a genuine dispersion strengthening mechanism operative at high temperature, attention has only recently turned to the details of the possible interactions between dislocations and hard, incoherent particles. Much insight has been gained by transmission electron microscopy of the dislocation configurations in creep-tested material. The field has also received theoretical support in the form of continuum-mechanics calculations of the high temperature effects on dislocation-particle forces. Finally, these elements have lead to a new model for dispersion strengthening which probably applies to most dispersion-hardened high-temperature materials.
Most significantly, the properties of the interface between the dispersoid particle and the matrix are found to be decisive for the properties of the material, as will be described below.

Transmission Electron Microscopy of Dislocation Configurations. The most detailed TEM study to date has not been performed on an aluminum alloy, but rather on a dispersion-strengthened nickel-base superalloy (30,31,32). This alloy was creep-deformed at about 80 % of its absolute solidus temperature and under stresses well below the Orowan stress of the particle dispersion. TEM micrographs show unambiguously that the dislocations are always captured in the process of detachment from the dispersoid after climb is completed.

TEM micrographs of the creep-tested aluminum alloys show in principle the same dislocation configurations (fig. 13). In particular, the dislocation interaction with the oxide particles can be well observed, whereas the more irregular morphology of the carbide dispersoids makes the interpretation of the dislocation contrast in the vicinity of the dispersoid difficult (compare fig. 9a). Thus, although the aluminum alloys studied are less well suited for a full quantitative evaluation of the micrographs, they suggest evidence that strengthening occurs by the same mechanism.

Overall, the TEM studies provide strong evidence that particle by-pass by climbing dislocations is indeed not controlled by the climb process but by a resistance to dislocation detachment from the dispersoids. In other words, the beneficial effect of dispersoid particles on high temperature creep would have to be attributed to an attractive particle-dislocation interaction.

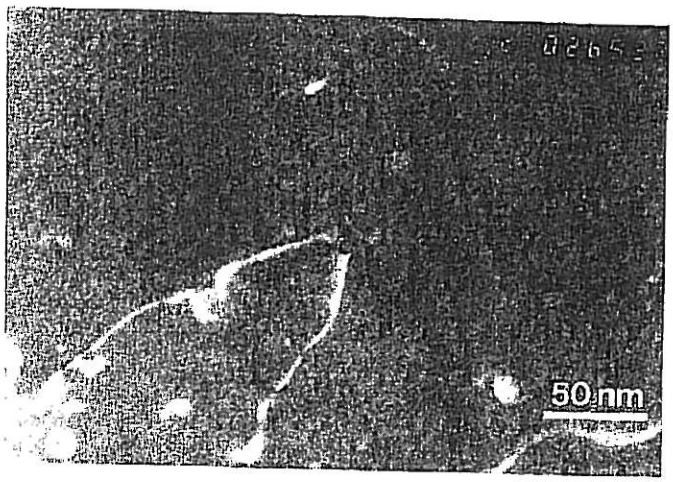


Figure 13 - TEM micrograph of dislocation-dispersoid configurations in A100, creep deformed at 673 K and $\dot{\varepsilon} = 1.0 \times 10^{-6}$ $s^{-1}$. An attractive interaction between dislocations and dispersoids is evident.

This conclusion is consistent with recent theoretical studies by Srolovitz et al. (33), who have shown that at high temperature the elastic interactions between particles and dislocations can be reversed: even an infinitely hard particle (which repels dislocations at low temperatures) will provide a strong attractive force, provided it is incoherent with the matrix. The reason is that slipping of and diffusion along the particle-matrix interface rapidly relaxes shear and, to some extent, hydrostatic stresses imposed on the particle by the approaching dislocation. This allows a lower line energy to be obtained in the vicinity of the interface, and leads to an attractive interaction.

Detachment-Controlled Dislocation Motion: A New Constitutive Equation for Dispersion-Strengthened High-Temperature Materials. When a dislocation climbs over a dispersoid particle which exerts an attractive force, it generally "feels" two types of barriers: When climbing up-hill, the dislocation line length increases, and the energy necessary has to be supplied by the external stress; down-hill climb occurs spontaneously at first, but then the dislocation runs up against the barrier to detachment from the dispersoid. The question which new arises is: under what condition does the detachment event assume control of the total by-pass process?

This problem has been treated by Arzt and Wilkinson (34), who calculate the back stress profiles for a dislocation climbing "locally" as a function of the strength of the attractive interaction. The results show that the first barrier leads to a "climb threshold" of the following form:

$$\sigma_c = 0.4\, \sigma_{Or}\, k^{5/2} \qquad (6)$$

The "detachment threshold" amounts to:

Figure 13 - TEM micrograph of dislocation-dispersoid configurations in AlCO, creep deformed at 673 K and $\dot{\varepsilon} = 1.0 \times 10^{-6}\ s^{-1}$. An attractive interaction between dislocations and dispersoids is evident.

This conclusion is consistent with recent theoretical studies by Srolovitz et al. (33), who have shown that at high temperature the elastic interactions between particles and dislocations can be reversed: even an infinitely hard particle (which repels dislocations at low temperatures) will provide a strong attractive force, provided it is incoherent with the matrix. The reason is that slipping of and diffusion along the particle-matrix interface rapidly relaxes shear and, to some extent, hydrostatic stresses imposed on the particle by the approaching dislocation. This allows a lower line energy to be obtained in the vicinity of the interface, and leads to an attractive interaction.

Detachment-Controlled Dislocation Motion: A New Constitutive Equation for Dispersion-Strengthened High-Temperature Materials. When a dislocation climbs over a dispersoid particle which exerts an attractive force, it generally "feels" two types of barriers: When climbing up-hill, the dislocation line length increases, and the energy necessary has to be supplied by the external stress; down-hill climb occurs spontaneously at first, but then the dislocation runs up against the barrier to detachment from the dispersoid. The question which new arises is: under what condition does the detachment event assume control of the total by-pass process?

This problem has been treated by Arzt and Wilkinson (34), who calculate the back stress profiles for a dislocation climbing "locally" as a function of the strength of the attractive interaction. The results show that the first barrier leads to a "climb threshold" of the following form:

$$\sigma_c = 0.1\ \sigma_{Or}\ k^{5/2} \qquad (6)$$

The "detachment threshold" amounts to:

$$\sigma_d = \sqrt{1-k^2}\ \sigma_{Or} \qquad (7)$$

The interaction strength is determined by the value of k, which is the ratio of the reduced line energy at the particle to that of a dislocation segment remote from the particle. For k = 1, no dislocation relaxation and thus no attractive interaction occurs, and the detachment threshold (eq. 7) vanishes; k = 0 signifies full relaxation, which results in the maximum detachment stress $\sigma_d = \sigma_{Or}$ and zero climb threshold (eq. 6).

In fig. 14, the two threshold stresses are displayed graphically as a function of k. The comparison illustrates an essential point: only a very modest attractive interaction, corresponding to a relaxation of about 6 % ($k \approx 0.94$), is required in order for dislocation detachment to become the event which controls the threshold stress. Recently, also a kinetic model for dislocation climb past an attractive particle has been developed (35). The theoretical predictions confirm that only attractive particles can produce a threshold stress behavior.

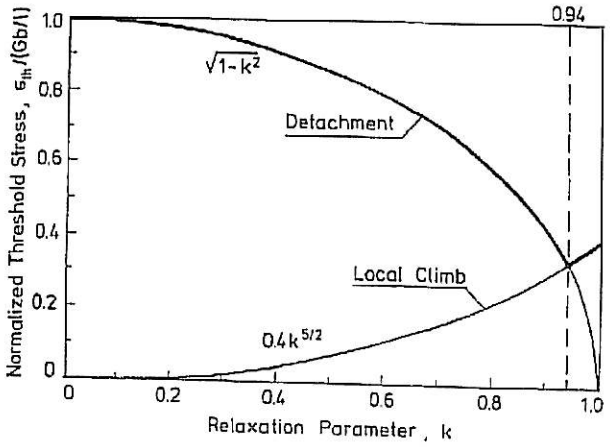


Figure 14 – Comparison of climb threshold with detachment threshold, as a function of the interaction parameter k (k = 1: no attraction, k = 0: maximum attraction). Only a small attractive interaction ($k \approx 0.94$) is required for the detachment threshold to control the dislocation motion.

Up to now the detachment threshold has been regarded as an "athermal" threshold stress. We therefore turn to the question how the detachment threshold can be affected by changes in temperature. To this end, the possibility of thermally-activated dislocation detachment must be considered. For spherical particles, the activation energy for detachment can be calculated rigorously (36); a suitable approximation is given by:

$$U = Gb^2 \cdot r\ [(1-k)(1-\sigma/\sigma_d)]^{3/2} \qquad (8)$$

where r is the particle radius and $\sigma_d$ the athermal detachment threshold. This expression goes to zero for k = 1 (no attraction) or $\sigma = \sigma_d$, as required.

If the detachment resistance is considered to be the only barrier to dislocation motion, then a constitutive equation can formally be obtained by inserting the activation energy in an Arrhenius expression (37):

$$\dot{\varepsilon} = \dot{\varepsilon}_o \cdot \exp\left\{ - \frac{Gb^2 r[(1-k)(1-\sigma/\sigma_d)]^{3/2}}{k_B T} \right\} \qquad (9)$$

Here, $\dot{\varepsilon}$ is the macroscopic strain rate, and $\dot{\varepsilon}_o$ an equivalent strain rate, e.g. the strain rate for k = 1 for which eq. 5 should be chosen.

The constitutive equation thus obtained differs formally from the semi-empirical expression eq. 3: it does not predict a "true" threshold stress but only a region of high stress sensitivity. From a fundamental point-of-view such a behavior is much more reasonable than a "true" deformation threshold: it is in agreement with the Second Law of Thermodynamics, according to which the rate of entropy production in a thermally activated system must always be non-zero. For practical applications, however, it can be shown that the constitutive equation approaches an equation of the form of eq. 3, with an "apparent" threshold stress which varies with temperature and with $\ell n\, \dot{\varepsilon}$.

Before leaving the area of micromechanistic modelling, it should be stressed that the account given above of the developments in theory has been necessarily brief. The interested reader is referred to the detailed publications cited in the text. Also, important further developments, such as the treatment of particle statistics by computer simulation, are still in progress.

## Interpretation of Creep Results on AlC Alloys

Now we return to the creep behavior of the dispersion-strengthened aluminum alloys described earlier in the text. An attempt will be made to interpret the results in the light of the theoretical developments outlined above.

The constitutive equation (eq. 9) contains the unknown k, whose value can be estimated by evaluating the actual creep data. One possibility is to match the theoretical and the experimental stress dependence of the creep rate (36). The results of this exercise are tabulated in table III.

Table III. Interaction factors k obtained by data evaluation

| Alloy | AlC0 | AlC2 | AlMg4C1 | AlFeCe |
|---|---|---|---|---|
| k at 573 K | 0.89 | 0.86 | 0.86 | 0.94 |

It is seen that the creep behavior of AlC0 can be explained by assuming that a dislocation experiences, on average, a reduction of its line energy in the vicinity of a dispersoid particle by 11 % (k = 0.89). Carbide dispersoids seem to be more efficient obstacles, achieving a reduction of about 14 % (k = 0.86 in AlC2, AlMg4C1).

It is instructive to apply this concept also to other high-temperature aluminum alloys. For example, the creep data of an Al-8.4Fe-3.6Ce alloy studied by Nix (23) can be readily interpreted when the interaction factor

is set to k = 0.94. This implies that the precipitates present in this rapidly solidified alloy appear to be only weakly attractive obstacles for dislocations. In such a case, thermally activated detachment of dislocations occurs easily, and a poorer high-temperature strength, compared to alloys with a stronger dispersoid-dislocation attraction, is predicted. This is consistent with the conclusion stated by Nix that the weakening of the alloy with increasing temperature is not due to thermal instability of the precipitates. In this particular fine-grained alloy, however, the contribution of the grain boundaries to the drop in strength is not totally clear. While the above interpretation should therefore be regarded as tentative, it illustrates a possible procedure for evaluating the potential of dispersion-strengthened high-temperature alloys: based on creep rate measurements, information on the effectiveness of dispersoid particles as dislocation obstacles at high temperature can in principle be obtained.

## Conclusion

The focus of this paper has been on reaction-milled aluminum alloys, whose high-temperature creep behavior has been investigated. An account has been given of recent developments in the theory of dispersion strengthening at high temperatures. While some details still need to be solved (e.g. influence of particle statistics), an attempt has been made to interpret the creep data in the light of a new model-based constitutive equation. It has been shown that this approach allows the creep behavior of dispersion strengthened alloys to be explained by ascribing a certain dislocation attraction effect to the dispersoid particles. Thus from macroscopic mechanical data, information on the effectiveness of the particle dispersion can be obtained.

These considerations also allow some qualitative conclusions on alloy design to be drawn. A trivial requirement is to aim for a high Orowan stress; this implies a small dispersoid spacing - possibly even smaller than what can be obtained by today's mechanical alloying techniques. There is a limit to the fineness of a particle dispersion which is set by the propensity to thermally-activated dislocation detachment from the dispersoids: the particles should generally be of the order of, say, 10 nm. A requirement which is in conflict with the need for not-too-small closely-spaced dispersoids is ductility, which decreases with increasing volume fraction of dispersoid.

In order to achieve optimum high-temperature strength in a dispersion-strengthened alloy, much attention should also be paid to the interface between the dispersoid particle and the matrix. This interface should allow maximum relaxation of a climbing dislocation, which points to a high interfacial energy. The "more coherent" a particle gets, the less efficient it becomes as an obstacle to dislocations at high temperatures. This explains why the high-temperature strengths achievable by coherent precipitates can never match those due to incoherent dispersoids, even when the precipitates are relatively stable.

Finally, when judging the potential of dispersion-strengthened materials for high-temperature applications, it should be realized that a drop in strength with increasing temperature can be due to at least three different effects: i) most trivial, thermal instability of the dispersoid particles, ii) a decreasing effectiveness of the dispersoid particles as dislocation obstacles at high temperatures, and iii) the onset of grain boundary processes. Item i) is often cited as an ad-hoc explanation for poor high-temperature strength, but does not always necessarily apply. Even a thermally stable particle dispersion may be unsuitable for high-temperature use be-

cause of an insufficient attractive interaction between dislocations and dispersoids (item ii). Finally, it should be remembered that a fine-grained structure is bound to lose its strength at high temperatures because of grain boundary sliding and/or damage formation. When these processes occur, the dispersion strengthening effect disappears in the alloy. This is also true for aluminum alloys (as has been shown above); when considering them for real high temperature applications, especially at low stresses and long expected life times, a grain-coarsening treatment may eventually be inevitable.

Acknowledgements. - The authors gratefully acknowledge the supply of specimens by Sintermetallwerk Krebsöge and Erbslöh Aluminium. This project is supported financially by the German Bundesministerium für Forschung und Technologie (project number 03M0010E4).

## References

1. R.F. Singer and E. Arzt, "Structure, Processing and Properties of ODS Superalloys", High Temperature Alloys for Gas Turbines and Other Applications 1986, eds. W. Betz, R. Brunetaud, D. Coutsouradis, H. Fischmeister, T. Gibbons, I. Kvernes, Y. Lindblom, J.B. Marriott, and D.B. Meadowcroft (Dordrecht: D. Reidel Publishing Company, 1986) 97-126.

2. E. Schmid, German Patents DRP 425451 and 425452 (1926).

3. R. Irmann, "SAP, Ein neuer Werkstoff der Pulvermetallurgie aus Aluminium", Techn. Rundschau (Bern), 41 (1949) 19.

4. A. v. Zeerleder, "Über Sintern von Aluminium-Legierungen", Z. Metallkunde., 41 (1950) 228-231.

5. A. v. Zeerleder, "Entwicklung und Stand von Sinteraluminium", Z. Metallkde., 46 (1955) 809-812.

6. J. Benjamin, "Dispersion Strengthened Superalloys by Mechanical Al-Alloying", Met. Trans., 1 (1970) 2943-2951.

7. G. Jangg and F. Kutner, "Herstellung und Eigenschaften von dispersionsgehärtetem Aluminium", Aluminium, 51 (1975) 641-645.

8. G. Jangg, "Dispersion Strengthened Al-$Al_4C_3$ Materials", Radex-Rundschau, 1986, 169-182.

9. J. Rösler and E. Arzt, "Microstructure and High Temperature Creep in Dispersion Strengthened Aluminum Alloys", to be published.

10. Y.W. Kim, W.M. Griffith, and F.H. Froes, "Surface Oxides in P/M Aluminium Alloys", J. Metals, 1985, 27-33.

11. G. Staniek, "Beobachtungen zur Rolle der Oxidhaut in pulvermetallurgisch hergestellten Aluminiumlegierungen", Aluminium, 60 (1984) 923-929.

12. R.F. Singer, W.C. Oliver, and W.D. Nix, "Identification of Dispersoid Phases Created in Aluminum during Mechanical Alloying", Met. Trans., 11A (1980) 1895-1901.

13. D.W. Dawe and J.S. Brammar, "The Microstructure of Aluminium-7% Aluminium Sintered Alloy (SAP)", J. Inst. Metals, 91 (1962-63) 222-223.

14. R.S. Goodrich and G.S. Ansell, "Transmission Electron Microscopy of Three Recrystallized Al-$Al_2O_3$ SAP-Type Alloys", Trans. Met. Soc. AIME, 230 (1964) 1372-1377.

15. A.S. Russell, Alcoa Research Labs, Techn. Paper No. 10, 1956.

16. W.C. Oliver and W.D. Nix, "High Temperature Deformation of Oxide Dispersion Strengthened Al and Al-Mg Solid Solutions", Acta Met., 30 (1982) 1335-1347.

17. M. v. Stackelberg und E. Schnorrenberg, "Die Struktur des Aluminiumcarbids $Al_4C_3$", Z. Phys. Chemie B, 27 (1934) 37-49.

18. A.K. Mukherjee, J.E. Bird, and J.E. Dorn, "Experimental Correlations for High-Temperature Creep", Trans ASM, 62 (1969) 155-179.

19. H.J. Frost and M.F. Ashby, Deformation Mechanism Maps (Oxford: Pergamon Press, 1982).

20. J.H. Gittus, "Theoretical Equation for Steady-State Dislocation Creep in a Material Having a Threshold Stress", Proc. Roy. Soc. A, 342 (1975) 279-287.

21. R.W. Lund and W.D. Nix, "High Temperature Creep of Ni-20Cr-2$ThO_2$ Single Crystals", Acta Met., 24 (1976) 469-481.

22. J.J. Stephens and W.D. Nix, "The Effect of Grain Morphology on Longitudinal Creep Properties of INCONEL MA 754 at Elevated Temperatures", Met. Trans., 16A (1985) 1307-1324.

23. W.D. Nix, "An Investigation of the Structure and High Temperature Mechanical Properties of Oxide Dispersion Strengthened Alloys", Report AFOSR-TR-85-0164, 1984.

24. P. Guyot, "Blocage des Dislocations dans les Alliages du Type S.A.P./Al-$Al_2O_3$", Acta Met., 12 (1964) 941-945.

25. G.S. Ansell and J. Weertman, "Creep of a Dispersion Hardened Aluminum Alloy", Trans. Met. Soc. AIME, 215 (1959) 838-843.

26. L.M. Brown and R.K. Ham, "Dislocation-Particle Interactions", Strengthening Methods in Crystals, eds. A. Kelly and R.B. Nicholson (Amsterdam: Elsevier, 1971), 9-135.

27. R.S.W. Shewfelt and L.M. Brown, "High-Temperature Strength of Dispersion-Hardened Single Crystals - II. Theory", Phil. Mag., 35 (1977) 945-962.

28. R. Lagneborg, "Bypassing of Dislocations Past Particles by a Climb Me-Mechanism", Scripta Met., 7 (1973) 605-613.

29. J. Rösler and E. Arzt, "The Kinetics of Dislocation Climb over Hard Particles: I. Climb without Attractive Particle-Dislocation Interaction, Acta Met., 36 (1988), in print.

30. J.H. Schröder and E. Arzt, "Weak Beam Studies of Dislocation/Dispersoid Interaction in an ODS Superalloy", Scripta Met., 19 (1985) 1129-1134.

31. J.H. Schröder, "Electron Microscopic Investigation of the High Temperature Mechanism in an ODS Superalloy", (Ph.D. Dissertation, Univ. Stuttgart, 1987), 148 pp.

32. V.C. Nardone and J.K. Tien, "Pinning of Dislocations on the Departure Side of Strengthening Dispersoids", Scripta Met., 17 (1983) 467-470.

33. D.J. Srolovitz et al., "Diffusionally Modified Dislocation-Particle Elastic Interactions", Acta Met., 32 (1984) 1079-1088.

34. E. Arzt and D.S. Wilkinson, "Threshold Stresses for Dislocation Climb over Hard Particles: The Effect of an Attractive Interaction", Acta Met., 34 (1986) 1893-1898.

35. E. Arzt and J. Rösler, "The Kinetics of Dislocation Climb over Hard Particles: II. Effects of an Attractive Interaction", Acta Met., 36 (1988), in print.

36. J. Rösler and E. Arzt, "A New Model-Based Constitutive Equation for Dispersion-Strengthened High-Temperature Materials", to be published.

37. A. Kelly and R.B. Nicholson, "Precipitation Hardening", Progr. Mat. Sci. Sci., 10 (1963) 151-391.